Eur. Phys. J. A (2024) 60:38
https://doi.org/10.1140/epja/s10050-024-01266-x

THE EUROPEAN PHYSICAL JOURNAL A

Regular Article - Theoretical Physics

Generic multi-particle transverse momentum correlations as a new tool for studying nuclear structure at the energy frontier

Emil Gorm Dahlbæk Nielsen, Frederik K. Rømer, Kristjan Gulbrandsen, You Zhou[a]

Niels Bohr Institute, University of Copenhagen, 2200 Copenhagen, Denmark

Received: 1 December 2023 / Accepted: 7 February 2024 / Published online: 22 February 2024

Communicated by Thomas DUGUET

Abstract The mean transverse momentum of produced particles, $[p_{\mathrm{T}}]$, and its event-by-event fluctuations give direct access to the initial conditions of ultra-relativistic heavy-ion collisions and help probe the colliding nuclei's structure. The $[p_{\mathrm{T}}]$ fluctuations can be studied via multi-particle p_{T} correlations; so far, only the lowest four orders have been studied. Higher-order fluctuations can provide stronger constraints on the initial conditions and improved sensitivity to the detailed nuclear structure; however, their direct implementation can be challenging and is still lacking. In this paper, we apply a generic recursive algorithm for the genuine multi-particle p_{T} correlations, which enables the accurate study of higher-order $[p_{\mathrm{T}}]$ fluctuations without heavy computational cost for the first time. With this algorithm, we will examine the power of multi-particle p_{T} correlations through Monte Carlo model studies with different nuclear structures. The impact on the nuclear structure studies, including the nuclear deformation and triaxial structure, will be discussed. These results demonstrate the usefulness of multi-particle p_{T} correlations for studying nuclear structure in high-energy nuclei collisions at RHIC and the LHC, which could serve as a complementary tool to existing low-energy nuclear structure studies.

1 Introduction

The primary goal of the heavy-ion collisions at ultra-relativistic energies, such as at the Relativistic Heavy Ion Collider (RHIC) and the Large Hadron Collider (LHC), is to create a quark-gluon plasma (QGP) and study its properties in the laboratory [1,2]. Experimental measurements of anisotropic flow [3,4] and its comparison to hydrodynamic model calculations [5–7], in particular via global Bayesian analysis [8,9], provide a powerful approach to constrain the specific about the specific viscosity of the QGP and its time evolution (temperature dependence). This represents the state-of-the-art understanding of the QGP [10]. However, the sizable uncertainty of the extracted QGP transport coefficients originates from poor knowledge about the initial conditions of heavy-ion collisions. A further reduction of this uncertainty can be achieved via in-depth investigations of the initial conditions [8,9]. Among various collective flow observables, the mean transverse momentum, $[p_{\mathrm{T}}]$, and its event-by-event fluctuations trace their origins to the initial state of the heavy-ion collision [11,12] and are arguably a more direct way than the approach of anisotropic flow to study the initial state fluctuations [13]. Several initial state properties have been proposed as good estimators of event-by-event mean transverse momentum fluctuations. These properties include the initial size R and the size fluctuations of the system that were introduced in [11], the transverse area of the overlap region and the initial eccentricity ϵ_2, introduced as A_e in [14], as well as the initial energy per unit rapidity at the initial time τ_0, E_i [15]. These estimators have been verified using hydrodynamic calculations that show E_i follows an approximate linear to the $[p_{\mathrm{T}}]$ [16]. Essentially, the $[p_{\mathrm{T}}]$ and its fluctuations reveal information about the fluctuations of the energy deposited in the initial state on an event-by-event basis.

It has been proposed that an improved understanding of the initial conditions of nuclei collisions leads to a more precise description of the geometrical shape of the overlapping colliding region [17]. In particular, for central collisions where the two colliding nuclei fully overlap, the spatial shape of the overlapping region could directly reflect the nuclear structure that existed before the collision occurred in the case of body-body collisions. Body-body collisions occur when the long axes of the nuclei are aligned with the beam direction, while tip-tip collisions occur when the short axes of the nuclei are aligned with the beam direction. It has also been shown that the imprint of the nuclear structure remains in the

[a] e-mail: you.zhou@cern.ch (corresponding author)

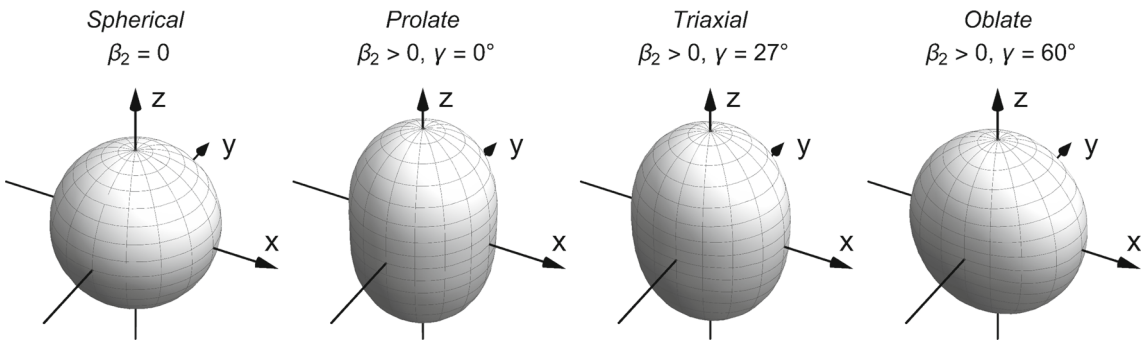

Fig. 1 Illustration of the surface of nuclei with different quadrupole deformation. From left to right: spherical, prolate, triaxial, and oblate

subsequent final state of the collective expansion, i.e., $[p_{\mathrm{T}}]$ fluctuations [18] and anisotropic flow [19], after the dynamic evolution of nucleus collisions. The study of nuclear structure is an important research topic in nuclear physics, as it reveals the fundamental properties and interactions of nucleons and nuclei. These studies allow us to test and improve the theoretical models and methods that describe the nuclear many-body problem, which remains a critical challenge from the low-energy side [17]. The imaging power of high-energy nucleus collisions provides a complementary approach to the existing low-energy nuclear structure study [20].

In the initial conditions of heavy-ion collisions, the nucleon positions are sampled from a modified Woods-Saxon distribution

$$\rho^{\mathrm{WS}}(r) = \frac{\rho_0}{1 + \exp\left(\frac{r - R(\theta,\varphi)}{a_0}\right)}. \tag{1}$$

The deformation of the nuclear surface is described by

$$R(\theta,\varphi) = R_0\left(1 + \beta_2\left[\cos\gamma\, Y_{20}(\theta,\varphi) + \sin\gamma\, Y_{22}(\theta,\varphi)\right]\right) \tag{2}$$

where R_0 is the nuclear radius, Y_{lm} are spherical harmonics, β_2 quantifies the strength of the quadrupole deformation, and the triaxial parameter γ controls the relative order of the three axes in the intrinsic frame of the nuclei. The impacts of β_2 and γ on the nuclear structure are illustrated in Fig. 1. Systematic studies of anisotropic flow using multi-particle azimuthal angle correlations show that several flow observables are sensitive to the nuclear quadrupole deformation β_2 [19]. However, none of the flow observables (in terms of azimuthal angle correlations) have the power to distinguish the triaxial structures [19], suggesting that different choices of observable may be needed to accomplish this, such as v_n^2-$[p_{\mathrm{T}}]$ correlations [21–24], or multi-particle p_{T} correlations [11,13].

This paper will present a generic recursive algorithm for the genuine multi-particle correlations (cumulants) of p_{T} in Sect. 2. The Monte Carlo models, introduced in Sect. 3, will be used to examine the power of multi-particle cumulants of p_{T}, with the results presented in Sect. 4. Finally, we will summarize in Sect. 5.

2 Algorithm for multi-particle p_{T} correlations

Multi-particle correlations have been a powerful tool in the study of heavy-ion collisions [25,26]. One successful example is using multi-particle azimuthal angle correlations to study the final state anisotropic particle expansion, quantified by anisotropic flow v_n [27,28]. Systematic studies of anisotropic flow, flow fluctuations, and flow correlations show that the selected flow observables are sensitive to the nuclear quadrupole deformation β_2 [19]. Still, none of the classical flow observables based on the azimuthal angle correlations has the power to distinguish the triaxial structures [19]. For the study of multi-particle p_{T} correlations, the lower orders have been available and used in the investigations of the initial conditions in heavy-ion collisions and also explored for their potential in the study of nuclear structure [18,29]. Meanwhile, when one manually derives the correlations, it is challenging and computationally demanding for the higher orders. A generic recursive algorithm provides an ideal solution. It has been successfully developed for multi-particle azimuthal correlations [28] and used in the above-mentioned anisotropic flow studies [19]. Following a similar idea, we propose a generic recursive algorithm for multi-particle $[p_{\mathrm{T}}]$ correlations in this paper.

In a single collision, many particles are produced. The averaged p_{T} correlation in this event is defined as

$$[p_{\mathrm{T}}^{(m)}] = \frac{\sum_{k_1\neq\cdots\neq k_m}^{M} w_{k_1}\cdot\ldots\cdot w_{k_m}\, p_{\mathrm{T},k_1}\cdot\ldots\cdot p_{\mathrm{T},k_m}}{\sum_{k_1\neq\cdots\neq k_m}^{M} w_{k_1}\cdot\ldots\cdot w_{k_m}}, \tag{3}$$

where M is the number of particles within a certain kinematic range in this event and w_{k_i} is a particle weight correcting for detector inefficiencies. Applying the constraint that

$k_1 \neq \ldots \neq k_m$ removes any auto-correlations such that the averaged p_{T} correlation measures the dynamic correlations due to event-by-event fluctuations and not the statistical correlations due to the finite number of tracks. The notation $[p_{\mathrm{T}}]$ is used for the mean transverse momentum calculated event-by-event within a certain kinematic range and is distinct from the mean transverse momentum, $\langle p_{\mathrm{T}} \rangle$, extrapolated to $p_{\mathrm{T}} = 0$ from spectra analyses over a large event ensemble [30]. Similar to the Generic Framework for azimuthal angle correlations [27,28], the numerator and denominator can be defined as

$$N\langle m \rangle_{p_{\mathrm{T}}} = \sum_{k_1 \neq \ldots \neq k_m}^{M} w_{k_1} \cdot \ldots \cdot w_{k_m} p_{\mathrm{T},k_1} \cdot \ldots \cdot p_{\mathrm{T},k_m}, \tag{4}$$

$$D\langle m \rangle_{p_{\mathrm{T}}} = \sum_{k_1 \neq \ldots \neq k_m}^{M} w_{k_1} \cdot \ldots \cdot w_{k_m}, \tag{5}$$

so that the averaged m-particle p_{T} correlation can be written as

$$[p_{\mathrm{T}}^{(m)}] = \frac{N\langle m \rangle_{p_{\mathrm{T}}}}{D\langle m \rangle_{p_{\mathrm{T}}}}. \tag{6}$$

The numerator and denominator in Eqs. (4) and (5), respectively, are calculated by constructing sums of different powers of the transverse momentum and particle weights

$$P_k = \sum_{i=1}^{M} w_i^k p_{\mathrm{T},i}^k \quad , \quad W_k = \sum_{i=1}^{M} w_i^k. \tag{7}$$

Unlike the previously done analyses of azimuthal angle correlations [27,28], the first-order p_{T} correlation does not vanish but is simply $[p_{\mathrm{T}}]$. The first few transverse momentum correlations are given by

$$[p_{\mathrm{T}}^{(1)}] = \frac{P_1}{W_1} = \frac{\sum_{i=1}^{M} w_i p_{\mathrm{T},i}}{\sum_{i=1}^{M} w_i} = [p_{\mathrm{T}}], \tag{8}$$

$$[p_{\mathrm{T}}^{(2)}] = \frac{P_1^2 - P_2}{W_1^2 - W_2}, \tag{9}$$

$$[p_{\mathrm{T}}^{(3)}] = \frac{P_1^3 - 3P_2P_1 + 2P_3}{W_1^3 - 3W_2W_1 + 2W_3} \tag{10}$$

$$[p_{\mathrm{T}}^{(4)}] = \frac{P_1^4 - 6P_2P_1^2 + 3P_2^2 + 8P_3P_1 - 6P_4}{W_1^4 - 6W_2W_1^2 + 3W_2^2 + 8W_3W_1 - 6W_4} \tag{11}$$

A general recursive formula can be constructed for Eqs. (4) and (5), allowing one to calculate a p_{T} correlation of any order from powers of P_k and W_k

$$N\langle m \rangle_{p_{\mathrm{T}}} = \sum_{k=1}^{m} (-1)^{k-1} N\langle m-k \rangle_{p_{\mathrm{T}}} \frac{(m-1)!}{(m-k)!} P_k \tag{12}$$

$$D\langle m \rangle_{p_{\mathrm{T}}} = \sum_{k=1}^{m} (-1)^{k-1} D\langle m-k \rangle_{p_{\mathrm{T}}} \frac{(m-1)!}{(m-k)!} W_k \tag{13}$$

where $N\langle 0 \rangle_{p_{\mathrm{T}}} \equiv 1$ and $D\langle 0 \rangle_{p_{\mathrm{T}}} \equiv 1$. Further written out applications of this recursive formula up to eighth order can be found in Appendix A.

The event-averaged p_{T} correlations correspond to the raw sample moments of the p_{T} distribution within some kinematic region

$$\langle [p_{\mathrm{T}}^{(m)}] \rangle = \frac{\sum_{\mathrm{events}} W'_m [p_{\mathrm{T}}^{(m)}]}{\sum_{\mathrm{events}} W'_m}, \tag{14}$$

where W'_m is an event weight. The choice of this weight here is $W'_m = D\langle m \rangle_{p_{\mathrm{T}}}$, which is the number of particle pairs similar to the weight used in anisotropic flow calculations to minimize the effects of multiplicity fluctuations. The higher-order moments contain contributions from the lower orders. The p_{T} cumulants, κ_m, (calculated from the correlations, $\langle [p_{\mathrm{T}}^{(m)}] \rangle$) reveal to which degree there exists a genuine p_{T} correlation amongst many particles (m) which cannot be factorized into correlations amongst fewer particles. A recursive formula for the mth-order cumulant [31] is given by

$$\kappa_m = \langle [p_{\mathrm{T}}^{(m)}] \rangle - \sum_{k=1}^{m-1} \binom{m-1}{k-1} \langle [p_{\mathrm{T}}^{(m-k)}] \rangle \kappa_k. \tag{15}$$

For the multi-particle p_{T} cumulants, considering the fact that the lower-order p_{T} correlations have been precisely subtracted by construction, they are expected to be insensitive to the few-particle correlations, such as the nonflow effects in the anisotropic flow studies, in the heavy-ion collisions. One can expand this formula by grouping common terms to get a formula solely dependent on powers of $\langle [p_{\mathrm{T}}^{(m)}] \rangle$. This has been done in Appendix B up to eighth order. These genuine correlations will be shown to be sensitive to the nuclear structure of the colliding nuclei.

3 Introduction to the theoretical models

In this paper, we will study the multi-particle transverse momentum correlations based on the simulations from two popular Monte Carlo models. The Heavy Ion Jet INteraction Generator, HIJING [32], is a Monte Carlo event generator for parton and particle production in high-energy nuclear collisions. Based on QCD-inspired models for multiple jet production, it incorporates mechanisms such as multiple mini-jet

Table 1 Simulated Xe–Xe collisions data sets in AMPT with four different configurations of the ^{129}Xe nuclear structure

Data set #	β_2	γ	a_0	# of events
1	0	0	0.57	$\sim$ 1 M
2	0.18	0	0.57	$\sim$ 1.5 M
3	0.18	27°	0.57	$\sim$ 2.5 M
4	0.18	60°	0.57	$\sim$ 2 M

production, soft excitation, nuclear shadowing of parton distribution functions, and jet interactions in dense hadronic matter. It has been reported that with the proper tuning, the HIJING model can describe particle production in high-energy proton-proton, proton-nucleus, and nucleus-nucleus collisions [32]. However, the HIJING model does not contain the proper mechanism to reproduce the anisotropic flow results in heavy-ion data [3]. Thus, the HIJING model is used to provide baseline predictions for the mean transverse momentum and its event-by-event fluctuations for heavy-ion collisions at the LHC.

Besides the HIJING model, A Multi-Phase Transport model, AMPT, is another popular Monte Carlo model that simulates nuclei collisions at relativistic energies [33]. The AMPT model run with String Melting consists of four main parts. First, the initial condition is based on the HIJING model [32], which describes how the nucleon distributions are arranged and moved inside the nuclei before they collide. Second, the Parton Cascade (ZPC) [34] simulates the partonic interactions inside the nuclei during the collision. Third, the hadronization, which is done via quark-coalescence [35], converts the partons into hadrons. Last, the hadronic interactions are modeled using the ART model [36]. The AMPT model can reproduce many experimental measurements from heavy-ion collisions, such as the production of various particle types and their collective behavior (the anisotropic flow). The AMPT model with default settings has difficulty reproducing the centrality dependence of $[p_{\mathrm{T}}]$ measurements in heavy-ion collisions at the LHC. Nevertheless, one can implement the nuclear structures in the initial state of the AMPT model. This allows one to examine if the imprint of the nuclear structure can be observed in the final state observables despite undergoing both partonic and hadronic interactions.

This paper implements four different settings for the ^{129}Xe structure. The parameters relevant to the nuclear structure studies are listed in Table 1, where the β_2 parameter of 0.18 is taken from [37] and the diffuseness parameter, a_0, is taken from [38]. The other input parameters in the AMPT model are kept fixed between the data sets. Like many previous AMPT model studies [19], the Lund string parameters are set to $a = 0.3$ and $b = 0.15$, the screening mass to $\mu = 2.2814$. The time-step is 0.2 fm, and the number of time steps for the hadronic interactions within ART is set to 150, which gives a hadron cascade time of 30 fm/c.

Following the idea established in [29], we consider the nuclei in a liquid-drop model with a sharp surface potential and in head-on collisions with a zero impact parameter. The mean transverse momentum is positively correlated with the gradient of nucleon density, $d_\perp$, in the overlapping region between the colliding nuclei

$$d_\perp = \sqrt{N_{\mathrm{part}}/S_\perp}, \tag{16}$$

where N_{part} is the number of nucleons participating in the collision and $S_\perp$ is the transverse area. Within the liquid-drop model, the dependence of the central moment of $d_\perp$ on the nuclear structure parameters can be roughly approximated by the following relation for a single event [29]

$$\frac{\delta d_\perp}{d_\perp} = \sqrt{\frac{5}{16\pi}}\beta_2\Big(\cos(\gamma)D^2_{0,0}(\Omega) + \frac{\sin(\gamma)}{\sqrt{2}}[D^2_{0,2}(\Omega) + D^2_{0,-2}(\Omega)]\Big), \tag{17}$$

where $D^2_{m,m'}$ are the elements of the Wigner D-matrix and Ω represents the Euler angles. The expressions for the higher-order central moments are obtained by integrating over the Euler angles

$$\left\langle\left(\frac{\delta d_\perp}{d_\perp}\right)^n\right\rangle = \beta_2^n\left(\frac{5}{16\pi}\right)^{n/2}\int\left(\cos(\gamma)D^2_{0,0} + \frac{\sin(\gamma)}{\sqrt{2}}[D^2_{0,2} + D^2_{0,-2}]\right)^n\frac{d\Omega}{8\pi^2} \tag{18}$$

from which the cumulants can be constructed, and the final cumulants of n-th order are scaled by $1/2^{n-1}$ to account for the independent orientations of the two nuclei. Table 2 shows the liquid-drop model estimates for the higher-order cumulants.

4 Results

Figure 2 shows the $\langle[p_{\mathrm{T}}]\rangle$ in Xe–Xe collisions at $\sqrt{s_{\mathrm{NN}}}$ = 5.44 TeV as a function of centrality. The top panel shows the $\langle[p_{\mathrm{T}}]\rangle$ for a spherical, prolate, triaxial, and oblate configuration of ^{129}Xe, and the bottom panel shows the ratio of $\langle[p_{\mathrm{T}}]\rangle$ in collisions of deformed nuclei against the $\langle[p_{\mathrm{T}}]\rangle$ calculated in collisions of spherical nuclei. The different ratios are consistent with unity suggesting that to first order, the transverse momentum cumulants are not a useful probe of the nuclear structure as the $\langle[p_{\mathrm{T}}]\rangle$ does not differ between the spherical ($\beta_2 = 0$), prolate ($\beta_2 = 0.18$), triaxial ($\beta_2 = 0.18, \gamma = 27°$), and oblate ($\beta_2 = 0.18$, $\gamma = 60°$) nuclei. This is consistent

Table 2 The cumulants of $d_\perp$ up to eighth order in a liquid-drop model potential averaged over random orientations. The first three entries are given in [29]

Final state Cumulant	Initial state Cumulant	Liquid-drop Model
κ_2	$\left\langle\left(\frac{\delta d_\perp}{d_\perp}\right)^2\right\rangle$	$\frac{1}{32\pi}\langle\beta_2^2\rangle$
κ_3	$\left\langle\left(\frac{\delta d_\perp}{d_\perp}\right)^3\right\rangle$	$\frac{\sqrt{5}}{896\pi^{3/2}}\langle\cos(3\gamma)\beta_2^3\rangle$
κ_4	$\left\langle\left(\frac{\delta d_\perp}{d_\perp}\right)^4\right\rangle - 3\cdot\left\langle\left(\frac{\delta d_\perp}{d_\perp}\right)^2\right\rangle^2$	$-\frac{3}{14336\pi^2}(7\langle\beta_2^2\rangle^2 - 5\langle\beta_2^4\rangle)$
κ_5	$\left\langle\left(\frac{\delta d_\perp}{d_\perp}\right)^5\right\rangle - 10\cdot\left\langle\left(\frac{\delta d_\perp}{d_\perp}\right)^3\right\rangle\cdot\left\langle\left(\frac{\delta d_\perp}{d_\perp}\right)^2\right\rangle$	$-\frac{5\sqrt{5}}{315392\pi^{5/2}}(11\langle\cos(3\gamma)\beta_2^3\rangle\langle\beta_2^2\rangle - 5\langle\beta_2^5\rangle)$
κ_6	$\left\langle\left(\frac{\delta d_\perp}{d_\perp}\right)^6\right\rangle - 15\cdot\left\langle\left(\frac{\delta d_\perp}{d_\perp}\right)^4\right\rangle\cdot\left\langle\left(\frac{\delta d_\perp}{d_\perp}\right)^2\right\rangle$	$\frac{5}{918412504\pi^3}(42042\langle\beta_2^2\rangle^3 - 5720\langle\cos(3\gamma)\beta_2^3\rangle^2$
	$+30\cdot\left\langle\left(\frac{\delta d_\perp}{d_\perp}\right)^2\right\rangle^3 - 10\cdot\left\langle\left(\frac{\delta d_\perp}{d_\perp}\right)^3\right\rangle^2$	$-45045\langle\beta_2^2\rangle\langle\beta_2^4\rangle + 8575\langle\beta_2^6\rangle + 700\langle\cos(6\gamma)\beta_2^6\rangle)$
κ_7	$\left\langle\left(\frac{\delta d_\perp}{d_\perp}\right)^7\right\rangle - 21\cdot\left\langle\left(\frac{\delta d_\perp}{d_\perp}\right)^5\right\rangle\cdot\left\langle\left(\frac{\delta d_\perp}{d_\perp}\right)^2\right\rangle$	$-\frac{15\sqrt{5}}{524812288}(2002\langle\beta_2^2\rangle^2\langle\cos(3\gamma)\beta_2^3\rangle$
	$+210\cdot\left\langle\left(\frac{\delta d_\perp}{d_\perp}\right)^3\right\rangle\cdot\left\langle\left(\frac{\delta d_\perp}{d_\perp}\right)^2\right\rangle^2$	$+715\langle\cos(3\gamma)\beta_2^3\rangle\langle\beta_2^4\rangle$
	$-35\cdot\left\langle\left(\frac{\delta d_\perp}{d_\perp}\right)^3\right\rangle\cdot\left\langle\left(\frac{\delta d_\perp}{d_\perp}\right)^4\right\rangle$	$+910\langle\cos(3\gamma)\beta_2^5\rangle\langle\beta_2^2\rangle - 175\cos(3\gamma)\beta_2^7\rangle)$
κ_8	$\left\langle\left(\frac{\delta d_\perp}{d_\perp}\right)^8\right\rangle - 28\cdot\left\langle\left(\frac{\delta d_\perp}{d_\perp}\right)^6\right\rangle\cdot\left\langle\left(\frac{\delta d_\perp}{d_\perp}\right)^2\right\rangle$	$\frac{5}{142748942336\pi^4}(2144142\langle\beta_2^2\rangle^4 - 3063060\langle\beta_2^2\rangle^2\langle\beta_2^4\rangle$
	$+420\cdot\left\langle\left(\frac{\delta d_\perp}{d_\perp}\right)^4\right\rangle\left\langle\left(\frac{\delta d_\perp}{d_\perp}\right)^2\right\rangle^2$	$-340\langle\beta_2^2\rangle\Big(2288\langle\cos(3\gamma)\beta_2^3\rangle^2 - 35\big(49\langle\beta_2^6\rangle$
	$-35\left\langle\left(\frac{\delta d_\perp}{d_\perp}\right)^4\right\rangle^2 - 630\cdot\left\langle\left(\frac{\delta d_\perp}{d_\perp}\right)^2\right\rangle^4$	$+4\langle\cos(6\gamma)\beta_2^6\rangle\big)\Big) + 25\Big(21879\langle\beta_2^4\rangle^2$
	$+560\cdot\left\langle\left(\frac{\delta d_\perp}{d_\perp}\right)^3\right\rangle^2\cdot\left\langle\left(\frac{\delta d_\perp}{d_\perp}\right)^2\right\rangle$	$+14144\langle\cos(3\gamma)\beta_2^3\rangle\langle\cos(3\gamma)\beta_2^5\rangle$
	$-56\cdot\left\langle\left(\frac{\delta d_\perp}{d_\perp}\right)^5\right\rangle\cdot\left\langle\left(\frac{\delta d_\perp}{d_\perp}\right)^3\right\rangle$	$-35\big(79\langle\beta_2^8\rangle + 16\langle\cos(6\gamma)\beta_2^8\rangle\big)\Big)$

with the expectation from the liquid-drop model; the integral in (18) yields zero when evaluated for $n = 1$.

The centrality dependence of $[p_T]$ fluctuations, in the form of the second-order cumulant or variance, κ_2, is shown in Fig. 3. The κ_2 result increases by about 10–15% in the central collisions for $\beta_2 \neq 0$ compared to the κ_2 for spherical nuclei. However, the results show no distinction between κ_2 calculations from prolate, triaxial, and oblate nuclei. This agrees with the expectation from the liquid-drop model, which predicts a positive contribution (an increase) in the second-order cumulant that is proportional to $\langle\beta_2^2\rangle$ and no sensitivity to the γ parameter, shown in Table 2. Therefore, we recommend that κ_2 should be considered as an additional probe to the anisotropic flow measurements [37] for constraining the parameter of ^{129}Xe. In particular, it should be included in the Bayesian fits on the experimental measurements to extract reliable deformation parameters from the high-energy heavy-ion collisions.

The centrality dependence of the third-order cumulant, κ_3, is shown in Fig. 4. The κ_3 is negative in the AMPT calculations compared to the positive κ_3 measured in experiments [39]. This difference is due to the choice of event weights introduced in Eq. 14. We used the number of particle pairs as the event weight in this AMPT calculation. This gives more significant weight to the events with more produced particles, typically tip-tip and body-body collisions, which better reflect the shape of the colliding nuclei. Moreover, applying the number of particle pairs weight is very helpful in minimizing the statistical uncertainties, as it gives a heavier weight to the events with more particle pairs [27]. Thus, we expect that this choice of weight enhances the sensitivity to the nuclear structure even though it might show some discrepancies with respect to the initial state estimations [29]. We have also tested the unit event weight in our AMPT calculations; it yields a positive κ_3 as the experimental measurements [39] but also leads to sizable statistical uncertainties that prevent us from drawing a confirmed conclusion of nuclear structure. As shown in Fig. 4, three distinct trends in central collisions, depending on the triaxiality parameter γ, are observed. Compared to the calculations from spher-

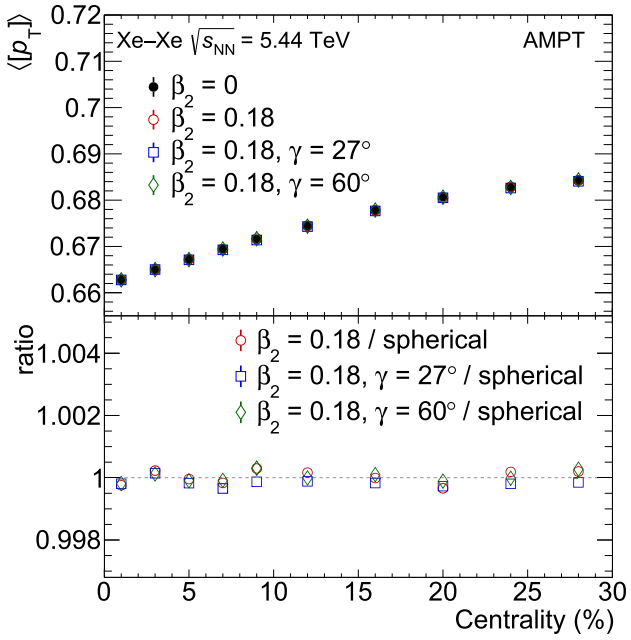

Fig. 2 The mean transverse momentum, $\langle[p_T]\rangle$, in Xe–Xe collisions at $\sqrt{s_{NN}}$ = 5.44 TeV as a function of centrality for four configurations of the nuclear structure simulated with the AMPT model

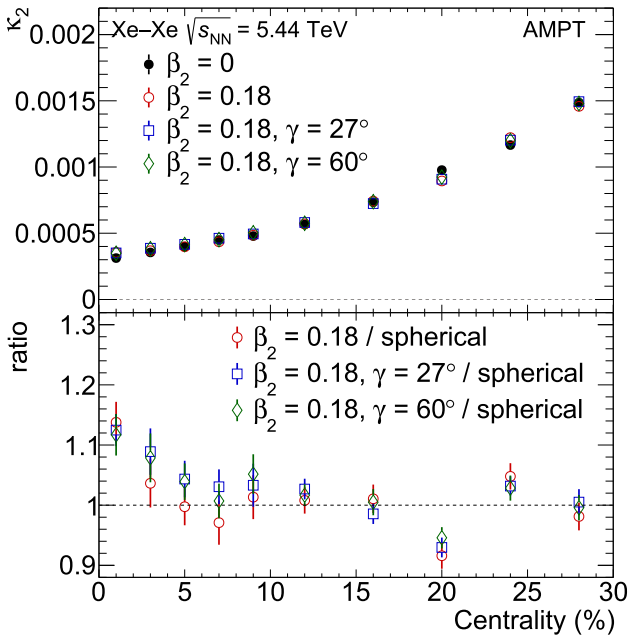

Fig. 3 The second-order mean transverse momentum cumulant, κ_2, in Xe–Xe collisions at $\sqrt{s_{NN}}$ = 5.44 TeV as a function of centrality for four configurations of the nuclear structure simulated with the AMPT model

ical nuclei, the magnitude of κ_3 is around 30% larger for oblate nuclei ($\gamma = 60°$) and around 30% smaller for prolate nuclei ($\gamma = 0°$) in central collisions albeit with large statistical uncertainties. The triaxial ^{129}Xe ($\gamma = 27°$) leads to a value of κ_3 consistent with the spherical case ($\beta_2 = 0$) in the 10% most central collisions. The emergence of the sensitivity to the triaxiality in κ_3 is unsurprising as triaxiality is a three-point structure, so a three-particle correlation is needed to measure it. This also explains why κ_2 can distinguish the overall quadrupole deformation ($\beta_2 = 0.18$) from the spherical case but offers no additional information: the two-particle κ_2 can only probe two axes of the nuclei at a time. In addition, the liquid-drop model predicts a positive contribution from the γ parameter in the prolate case ($\cos(3\gamma) = 1$), zero contribution from fully triaxial ($\cos(3\gamma) = 0$), and negative contribution from the oblate case ($\cos(3\gamma) = -1$). The AMPT calculations follow the same trend. However, as the κ_3 values are negative, the ordering of the points with different γ parameters is inverted in the ratio plot, shown in the bottom panel of Fig. 4. The above results further underline the importance of κ_3 in exploring triaxial nuclear structure. It suggests that not only the correlations between p_T and v_2^2, which have been widely used [23,40,41] but also the third order $[p_T]$ fluctuations in central collisions should be considered in the comparisons between model calculations and experimental measurements from the LHC experiments.

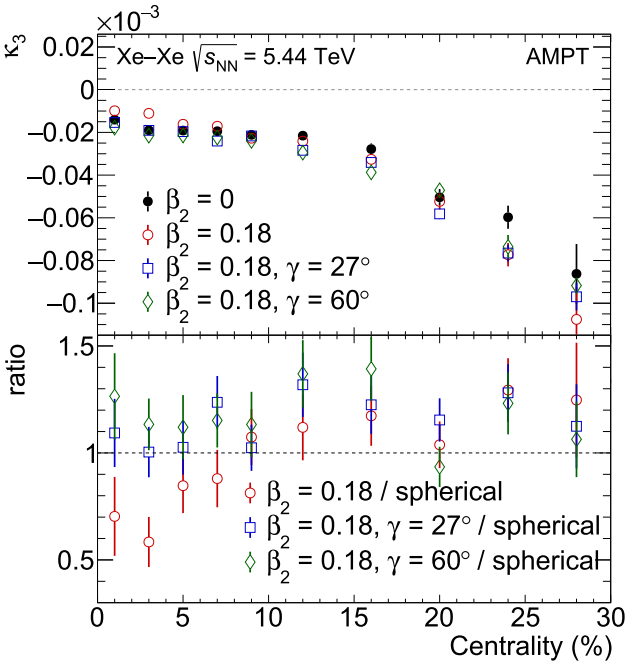

Fig. 4 The third-order mean transverse momentum cumulant, κ_3, in Xe–Xe collisions at $\sqrt{s_{NN}}$ = 5.44 TeV as a function of centrality for four configurations of the nuclear structure simulated with the AMPT model

Figure 5 shows the centrality dependence of the fourth-order cumulant, κ_4, and the comparison between the different nuclear structures. Similar to κ_3, κ_4 results are also obtained using the number of particle pair weights; the results can distinguish between different triaxial shapes in central collisions despite sizable uncertainties. The collisions of oblate nuclei yield the largest κ_4 in central collisions. The κ_4 for the triaxial case is smaller than the oblate case but larger than for

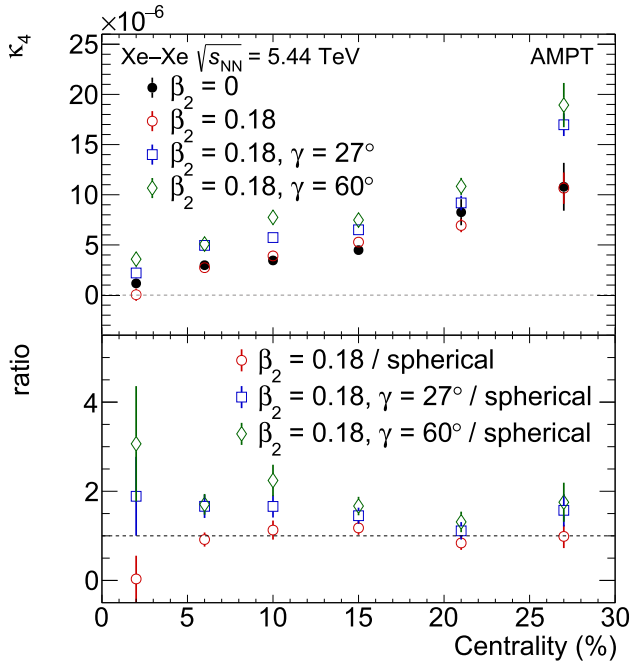

Fig. 5 The fourth-order mean transverse momentum cumulant, κ_4, in Xe–Xe collisions at $\sqrt{s_{\rm NN}}$ = 5.44 TeV as a function of centrality for four configurations of the nuclear structure simulated with the AMPT model

spherical nuclei. The prolate nuclei yield the smallest κ_4 in central collisions, almost a 100% difference with respect to the spherical case. This does not match the prediction from the simple liquid-drop model, where the fourth-order cumulant is expected to be proportional to some combination of the moments of β_2 only. However, a dependence of the initial state cumulant $(\delta d_\perp/d_\perp)^4 - 3(\delta d_\perp/d_\perp)^2$ on the γ parameter is also seen in MC-Glauber simulations of various deformed collision systems [29]. The ordering of the calculations in the bottom plot of Fig. 5 is similar to that in Fig. 4 (bottom), but in this case, the ordering is not inverted, suggesting that γ either has an opposite contribution to κ_4 compared to κ_3 or that the γ affects the magnitude of the cumulants. That κ_4 is sensitive to the γ parameter is surprising based on the leading-order approximation of the liquid-drop model, and it would be interesting to see whether κ_4 exhibits similar sensitivity within hydrodynamic models.

The predictions for the various orders of κ_n $(n \leq 8)$ are given with the HIJING model in Fig. 6. Servicing as the baseline for the experiments, the unit weight is used in this HIJING calculation, and no special consideration of the nuclear structure has been applied. Within the HIJING model, the fluctuations of the transverse momentum follow that of a superposition of independent sources, which can be both short- and long-range in nature [18,42]. The first three orders of cumulants, $\kappa_1 - \kappa_3$, are found to be strictly positive across the centrality range, which qualitatively agrees with the recent experimental measurements [39]. κ_4 is positive in central collisions, changes sign in semi-central collisions and then becomes positive again above 30% centrality. The higher-order cumulants ($n > 4$) fluctuate around zero in central and semi-central collisions, except κ_6, which is strictly negative. The non-zero higher-order cumulants suggest that the fluctuations of the mean transverse momentum are not trivial even in heavy-ion collisions viewed as a superposition of pp collisions.

5 Summary

Multi-particle correlations and cumulants of transverse momentum constrain the size and size fluctuations in the initial conditions of heavy-ion collisions, making them an ideal probe of the nuclear structure of colliding nuclei at ultra-relativistic colliders. This paper proposes a new generic algorithm of multi-particle $p_{\rm T}$ correlations that enables an efficient and precise study of $p_{\rm T}$ fluctuations up to arbitrary orders. Using the AMPT transport model with various settings of nuclear structure, including spherical, prolate, triaxial, and oblate shapes of ^{129}Xe, we investigate the impact of nuclear structure on the first four orders of $[p_{\rm T}]$ fluctuations. We find that at first order, the $p_{\rm T}$ cumulants are insensitive to the nuclear structure and that at least second order is required to probe the deformation of the colliding nuclei. The variance, κ_2, shows a β_2-dependent increase in central collisions but cannot distinguish between the prolate, triaxial, or oblate cases consistent with the expectation from the simple liquid-drop model. The third- and fourth-order cumulants, κ_3 and κ_4, show a γ-dependent splitting of the calculated values in the most central collisions with opposite contributions. The γ-dependence of κ_4 is not expected from the liquid-drop model prediction, suggesting that a more complex model of the interplay between nuclear structure and size fluctuations is necessary to understand this effect.

These studies show the impact of nuclear structure on the $[p_{\rm T}]$ fluctuations and how they can be utilized to probe the shape of the colliding nuclei at the energy frontier (at the level of TeV). The $p_{\rm T}$ cumulants are, through their relation to the size fluctuations, coupled to the moments of the deformation parameters. Further study of these relations and measurements of the cumulants at experiments such as those at the LHC can introduce a new avenue for studying nuclear structure in high-energy heavy-ion collisions, which is complementary to existing low-energy measurements and can serve as experimental validation of low-energy theoretical predictions. Furthermore, including the $p_{\rm T}$ cumulants as experimental inputs in Bayesian analyses can provide independent constraints on the deformation parameters.

The study of nuclear structure with heavy-ion collisions is an evolving field, and the presented method and observables can provide a useful approach in potential future runs

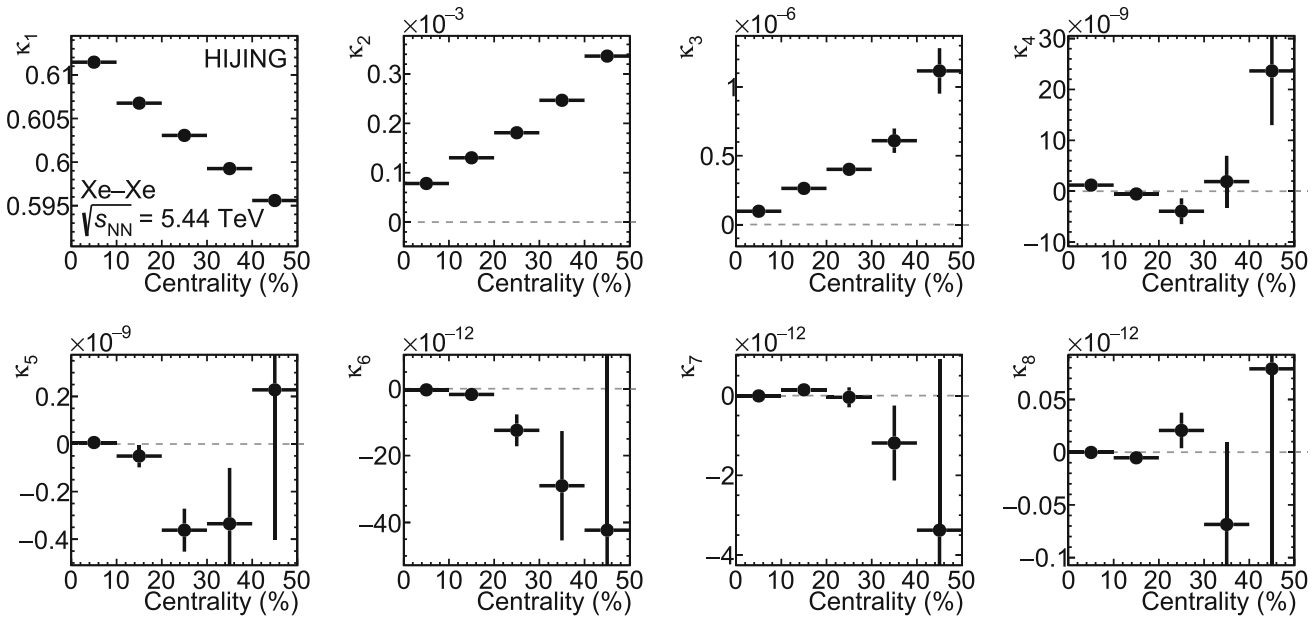

Fig. 6 The cumulants of the mean transverse momentum, κ_n ($n \leq 8$), in Xe–Xe collisions at $\sqrt{s_{\rm NN}} = 5.44$ TeV as a function of centrality simulated with the HIJING model

of deformed nuclei species at the LHC to constrain the shape of nuclei across the nuclide chart.

Acknowledgements We thank Chunjian Zhang for his help on the AMPT code and Anna Ingmer Boye for her initial contributions to the work. The authors are funded by the European Union (ERC, Initial-Conditions), VILLUM FONDEN (Grant Number 00025462), and Danmarks Frie Forskningsfond (Independent Research Fund Denmark). We thank the participants of the EMMI Rapid Reaction Task Force "Nuclear Physics Confronts Relativistic Collisions of Isobars" and the ESNT workshop "Deciphering Nuclear Phenomenology across Energy Scales" for fruitful discussions.

Funding Open access funding provided by Copenhagen University.

Data Availability Statement The manuscript has associated data in a data repository [Authors' comment: [Authors' comment: Data are available upon request].

Appendix A: Multi-particle $p_{\rm T}$ correlations

$$[p_{\rm T}^{(1)}] = \frac{P_1}{W_1} \tag{A.1}$$

$$[p_{\rm T}^{(2)}] = \frac{P_1^2 - P_2}{W_1^2 - W_2} \tag{A.2}$$

$$[p_{\rm T}^{(3)}] = \frac{P_1^3 - 3P_2P_1 + 2P_3}{W_1^3 - 3W_2W_1 + 2W_3} \tag{A.3}$$

$$[p_{\rm T}^{(4)}] = \frac{P_1^4 - 6P_2P_1^2 + 3P_2^2 + 8P_3P_1 - 6P_4}{W_1^4 - 6W_2W_1^2 + 3W_2^2 + 8W_3W_1 - 6W_4} \tag{A.4}$$

$$\begin{aligned}[p_{\rm T}^{(5)}] = {} & \Big[P_1^5 - 10P_2P_1^3 + 15P_2^2P_1 \\ & + 20P_3P_1^2 - 20P_3P_2 - 30P_4P_1 + 24P_5\Big] \\ & / \Big[W_1^5 - 10W_2W_1^3 + 15W_2^2W_1 + 20W_3W_1^2 \\ & - 20W_3W_2 - 30W_4W_1 + 24W_5\Big]\end{aligned} \tag{A.5}$$

$$\begin{aligned}[p_{\rm T}^{(6)}] = {} & \Big[P_1^6 - 15P_2P_1^4 + 45P_1^2P_2^2 \\ & - 15P_2^3 + 40P_3P_1^3 - 120P_3P_2P_1 \\ & + 40P_3^2 - 90P_4P_1^2 + 90P_4P_2 \\ & + 144P_5P_1 - 120P_6\Big] / \Big[W_1^6 - \\ & 15W_2W_1^4 + 45W_1^2W_2^2 - 15W_2^3 \\ & + 40W_3W_1^3 - 120W_3W_2W_1 \\ & + 40W_3^2 - 90W_4W_1^2 + 90W_4W_2\end{aligned}$$

$$+ 144W_5W_1 - 120W_6\Big] \tag{A.6}$$

$$\begin{aligned}[p_{\mathrm{T}}^{(7)}] = \Big[&P_1^7 - 21P_2P_1^5 + 105P_1^3P_2^2 \\ &- 105P_2^3P_1 + 70P_3P_1^4 - 420P_3P_2P_1^2 \\ &+ 210P_3P_2^2 + 280P_3^2P_1 - 210P_4P_1^3 \\ &+ 630P_4P_2P_1 - 420P_4P_3 + 504P_5P_1^2 \\ &- 504P_5P_2 - 840P_6P_1 + 720P_7\Big]/\Big[W_1^7 \\ &- 21W_2W_1^5 + 105W_1^3W_2^2 \\ &- 105W_2^3W_1 + 70W_3W_1^4 - 420W_3W_2W_1^2 \\ &+ 210W_3W_2^2 + 280W_3^2W_1 - 210W_4W_1^3 \\ &+ 630W_4W_2W_1 - 420W_4W_3 + 504W_5W_1^2 \\ &- 504W_5W_2 - 840W_6W_1 + 720W_7\Big]\end{aligned} \tag{A.7}$$

$$\begin{aligned}[p_{\mathrm{T}}^{(8)}] = \Big[&P_1^8 - 28P_2P_1^6 + 210P_2^2P_1^4 \\ &- 420P_2^3P_1^2 + 105P_2^4 + 112P_3P_1^5 \\ &- 1120P_3P_2P_1^3 + 1680P_3P_2^2P_1 + 1120P_3^2P_1^2 \\ &- 1120P_3^2P_2 - 420P_4P_1^4 + 2520P_4P_2P_1^2 \\ &- 1260P_4P_2^2 - 3360P_4P_3P_1 + 1260P_4^2 \\ &+ 1344P_5P_1^3 - 4032P_5P_2P_1 + 2688P_5P_3 \\ &- 3360P_6P_1^2 + 3360P_6P_2 + 5760P_7P_1 \\ &- 5040P_8\Big]/\Big[W_1^8 - 28W_2W_1^6 + 210W_2^2W_1^4 \\ &- 420W_2^3W_1^2 + 105W_2^4 + 112W_3W_1^5 \\ &- 1120W_3W_2W_1^3 + 1680W_3W_2^2W_1 + 1120W_3^2W_1^2 \\ &- 1120W_3^2W_2 - 420W_4W_1^4 + 2520W_4W_2W_1^2 \\ &- 1260W_4W_2^2 - 3360W_4W_3W_1 + 1260W_4^2 \\ &+ 1344W_5W_1^3 - 4032W_5W_2W_1 + 2688W_5W_3 \\ &- 3360W_6W_1^2 + 3360W_6W_2 + 5760W_7W_1 \\ &- 5040W_8\Big]\end{aligned} \tag{A.8}$$

Appendix B: Multi-particle p_{T} cumulants

$$\kappa_1 = \langle[p_{\mathrm{T}}]\rangle \tag{B.9}$$

$$\kappa_2 = \langle[p_{\mathrm{T}}^{(2)}]\rangle - \langle[p_{\mathrm{T}}]\rangle^2 \tag{B.10}$$

$$\kappa_3 = \langle[p_{\mathrm{T}}^{(3)}]\rangle - 3\langle[p_{\mathrm{T}}^{(2)}]\rangle\langle[p_{\mathrm{T}}]\rangle + 2\langle[p_{\mathrm{T}}]\rangle^3 \tag{B.11}$$

$$\begin{aligned}\kappa_4 = &\langle[p_{\mathrm{T}}^{(4)}]\rangle - 4\langle[p_{\mathrm{T}}^{(3)}]\rangle\langle[p_{\mathrm{T}}]\rangle - 3\langle[p_{\mathrm{T}}^{(2)}]\rangle^2 \\ &+ 12\langle[p_{\mathrm{T}}^{(2)}]\rangle\langle[p_{\mathrm{T}}]\rangle^2 - 6\langle[p_{\mathrm{T}}]\rangle^4\end{aligned} \tag{B.12}$$

$$\begin{aligned}\kappa_5 = &\langle[p_{\mathrm{T}}^{(5)}]\rangle - 5\langle[p_{\mathrm{T}}^{(4)}]\rangle\langle[p_{\mathrm{T}}]\rangle - 10\langle[p_{\mathrm{T}}^{(3)}]\rangle\langle[p_{\mathrm{T}}^{(2)}]\rangle \\ &+ 30\langle[p_{\mathrm{T}}^{(2)}]\rangle^2\langle[p_{\mathrm{T}}]\rangle + 20\langle[p_{\mathrm{T}}^{(3)}]\rangle\langle[p_{\mathrm{T}}]\rangle^2 \\ &- 60\langle[p_{\mathrm{T}}^{(2)}]\rangle\langle[p_{\mathrm{T}}]\rangle^3 + 24\langle[p_{\mathrm{T}}]\rangle^5\end{aligned} \tag{B.13}$$

$$\begin{aligned}\kappa_6 = &\langle[p_{\mathrm{T}}^{(6)}]\rangle - 6\langle[p_{\mathrm{T}}^{(5)}]\rangle\langle[p_{\mathrm{T}}]\rangle - 15\langle[p_{\mathrm{T}}^{(4)}]\rangle\langle[p_{\mathrm{T}}^{(2)}]\rangle \\ &- 10\langle[p_{\mathrm{T}}^{(3)}]\rangle^2 + 30\langle[p_{\mathrm{T}}^{(2)}]\rangle^3 + 30\langle[p_{\mathrm{T}}^{(4)}]\rangle\langle[p_{\mathrm{T}}]\rangle^2 \\ &+ 120\langle[p_{\mathrm{T}}^{(3)}]\rangle\langle[p_{\mathrm{T}}^{(2)}]\rangle\langle[p_{\mathrm{T}}]\rangle - 270\langle[p_{\mathrm{T}}^{(2)}]\rangle^2\langle[p_{\mathrm{T}}]\rangle^2 \\ &- 120\langle[p_{\mathrm{T}}^{(3)}]\rangle\langle[p_{\mathrm{T}}]\rangle^3 + 360\langle[p_{\mathrm{T}}^{(2)}]\rangle\langle[p_{\mathrm{T}}]\rangle^4 \\ &- 120\langle[p_{\mathrm{T}}]\rangle^6\end{aligned} \tag{B.14}$$

$$\begin{aligned}\kappa_7 = &\langle[p_{\mathrm{T}}^{(7)}]\rangle - 7\langle[p_{\mathrm{T}}^{(6)}]\rangle\langle[p_{\mathrm{T}}]\rangle - 21\langle[p_{\mathrm{T}}^{(5)}]\rangle\langle[p_{\mathrm{T}}^{(2)}]\rangle \\ &+ 42\langle[p_{\mathrm{T}}^{(5)}]\rangle\langle[p_{\mathrm{T}}]\rangle^2 - 35\langle[p_{\mathrm{T}}^{(4)}]\rangle\langle[p_{\mathrm{T}}^{(3)}]\rangle \\ &+ 210\langle[p_{\mathrm{T}}^{(4)}]\rangle\langle[p_{\mathrm{T}}^{(2)}]\rangle\langle[p_{\mathrm{T}}]\rangle - 210\langle[p_{\mathrm{T}}^{(4)}]\rangle\langle[p_{\mathrm{T}}]\rangle^3 \\ &+ 140\langle[p_{\mathrm{T}}^{(3)}]\rangle^2\langle[p_{\mathrm{T}}]\rangle + 210\langle[p_{\mathrm{T}}^{(3)}]\rangle\langle[p_{\mathrm{T}}^{(2)}]\rangle^2 \\ &- 1260\langle[p_{\mathrm{T}}^{(3)}]\rangle\langle[p_{\mathrm{T}}^{(2)}]\rangle\langle[p_{\mathrm{T}}]\rangle^2 + 840\langle[p_{\mathrm{T}}^{(3)}]\rangle\langle[p_{\mathrm{T}}]\rangle^4 \\ &- 630\langle[p_{\mathrm{T}}^{(2)}]\rangle^3\langle[p_{\mathrm{T}}]\rangle + 2520\langle[p_{\mathrm{T}}^{(2)}]\rangle^2\langle[p_{\mathrm{T}}]\rangle^3 \\ &- 2520\langle[p_{\mathrm{T}}^{(2)}]\rangle\langle[p_{\mathrm{T}}]\rangle^5 + 720\langle[p_{\mathrm{T}}]\rangle^7\end{aligned} \tag{B.15}$$

$$\begin{aligned}\kappa_8 = &\langle[p_{\mathrm{T}}^{(8)}]\rangle - 8\langle[p_{\mathrm{T}}^{(7)}]\rangle\langle[p_{\mathrm{T}}]\rangle \\ &- 28\langle[p_{\mathrm{T}}^{(6)}]\rangle\langle[p_{\mathrm{T}}^{(2)}]\rangle + 56\langle[p_{\mathrm{T}}^{(6)}]\rangle\langle[p_{\mathrm{T}}]\rangle^2 \\ &- 56\langle[p_{\mathrm{T}}^{(5)}]\rangle\langle[p_{\mathrm{T}}^{(3)}]\rangle + 336\langle[p_{\mathrm{T}}^{(5)}]\rangle\langle[p_{\mathrm{T}}^{(2)}]\rangle\langle[p_{\mathrm{T}}]\rangle \\ &- 336\langle[p_{\mathrm{T}}^{(5)}]\rangle\langle[p_{\mathrm{T}}]\rangle^3 - 35\langle[p_{\mathrm{T}}^{(4)}]\rangle^2 \\ &+ 560\langle[p_{\mathrm{T}}^{(4)}]\rangle\langle[p_{\mathrm{T}}^{(3)}]\rangle\langle[p_{\mathrm{T}}]\rangle + 420\langle[p_{\mathrm{T}}^{(2)}]\rangle^2\langle[p_{\mathrm{T}}^{(4)}]\rangle \\ &- 2520\langle[p_{\mathrm{T}}^{(4)}]\rangle\langle[p_{\mathrm{T}}^{(2)}]\rangle\langle[p_{\mathrm{T}}]\rangle^2 + 1680\langle[p_{\mathrm{T}}^{(4)}]\rangle\langle[p_{\mathrm{T}}]\rangle^4 \\ &+ 560\langle[p_{\mathrm{T}}^{(3)}]\rangle^2\langle[p_{\mathrm{T}}^{(2)}]\rangle - 1680\langle[p_{\mathrm{T}}^{(3)}]\rangle^2\langle[p_{\mathrm{T}}]\rangle^2 \\ &- 5040\langle[p_{\mathrm{T}}^{(3)}]\rangle\langle[p_{\mathrm{T}}^{(2)}]\rangle^2\langle[p_{\mathrm{T}}]\rangle \\ &+ 13440\langle[p_{\mathrm{T}}^{(3)}]\rangle\langle[p_{\mathrm{T}}^{(2)}]\rangle\langle[p_{\mathrm{T}}]\rangle^3 \\ &- 6720\langle[p_{\mathrm{T}}^{(3)}]\rangle\langle[p_{\mathrm{T}}]\rangle^5 - 630\langle[p_{\mathrm{T}}^{(2)}]\rangle^4 \\ &+ 10080\langle[p_{\mathrm{T}}^{(2)}]\rangle^3\langle[p_{\mathrm{T}}]\rangle^2 - 25200\langle[p_{\mathrm{T}}^{(2)}]\rangle^2\langle[p_{\mathrm{T}}]\rangle^4 \\ &+ 20160\langle[p_{\mathrm{T}}^{(2)}]\rangle\langle[p_{\mathrm{T}}]\rangle^6 - 5040\langle[p_{\mathrm{T}}]\rangle^8\end{aligned} \tag{B.16}$$

References

1. E.V. Shuryak, Quantum chromodynamics and the theory of Superdense matter. Phys. Rept. **61**, 71–158 (1980). https://doi.org/10.1016/0370-1573(80)90105-2
2. E.V. Shuryak, Quark-Gluon plasma and hadronic production of Leptons, Photons and Psions. Phys. Lett. **78B**, 150 (1978). https://doi.org/10.1016/0370-2693(78)90370-2. (**[Yad. Fiz.28,796(1978)]**)
3. ALICE Collaboration, K. Aamodt et al., Higher harmonic anisotropic flow measurements of charged particles in Pb–Pb collisions at $\sqrt{s_{\mathrm{NN}}}$ = 2.76 TeV. Phys. Rev. Lett. **107**, 032301 (2011). https://doi.org/10.1103/PhysRevLett.107.032301, arXiv:1105.3865 [nucl-ex]
4. A.L.I.C.E. Collaboration, J. Adam et al., Anisotropic flow of charged particles in Pb-Pb collisions at $\sqrt{s_{\mathrm{NN}}}$ = 5.02 TeV. Phys. Rev. Lett. **116**(13), 132302 (2016). https://doi.org/10.1103/PhysRevLett.116.132302. arXiv:1602.01119 [nucl-ex]
5. B. Muller, J. Schukraft, B. Wyslouch, First Results from Pb+Pb collisions at the LHC. Ann. Rev. Nucl. Part. Sci. **62**, 361–386

(2012). https://doi.org/10.1146/annurev-nucl-102711-094910. arXiv:1202.3233 [hep-ex]
6. U. Heinz, R. Snellings, Collective flow and viscosity in relativistic heavy-ion collisions. Ann. Rev. Nucl. Part. Sci. **63**, 123–151 (2013). https://doi.org/10.1146/annurev-nucl-102212-170540. arXiv:1301.2826 [nucl-th]
7. H. Song, Y. Zhou, K. Gajdosova, Collective flow and hydrodynamics in large and small systems at the LHC. Nucl. Sci. Tech. **28**(7), 99 (2017). https://doi.org/10.1007/s41365-017-0245-4. arXiv:1703.00670 [nucl-th]
8. J.E. Bernhard, J.S. Moreland, S.A. Bass, Bayesian estimation of the specific shear and bulk viscosity of quark-gluon plasma. Nat. Phys. **15**(11), 1113–1117 (2019). https://doi.org/10.1038/s41567-019-0611-8
9. J.E.T.S.C.A.P.E. Collaboration, D. Everett et al., Multisystem Bayesian constraints on the transport coefficients of QCD matter. Phys. Rev. C **103**(5), 054904 (2021). https://doi.org/10.1103/PhysRevC.103.054904. arXiv:2011.01430 [hep-ph]
10. ALICE Collaboration, The ALICE experiment—a journey through QCD. arXiv:2211.04384 [nucl-ex]
11. W. Broniowski, M. Chojnacki, L. Obara, Size fluctuations of the initial source and the event-by-event transverse momentum fluctuations in relativistic heavy-ion collisions. Phys. Rev. C **80**, 051902 (2009). https://doi.org/10.1103/PhysRevC.80.051902. arXiv:0907.3216 [nucl-th]
12. P. Bozek, W. Broniowski, Transverse-momentum fluctuations in relativistic heavy-ion collisions from event-by-event viscous hydrodynamics. Phys. Rev. C **85**, 044910 (2012). https://doi.org/10.1103/PhysRevC.85.044910. arXiv:1203.1810 [nucl-th]
13. G. Giacalone, F.G. Gardim, J. Noronha-Hostler, J.-Y. Ollitrault, Skewness of mean transverse momentum fluctuations in heavy-ion collisions. Phys. Rev. C **103**(2), 024910 (2021). https://doi.org/10.1103/PhysRevC.103.024910. arXiv:2004.09799 [nucl-th]
14. B. Schenke, C. Shen, D. Teaney, Transverse momentum fluctuations and their correlation with elliptic flow in nuclear collision. Phys. Rev. C **102**(3), 034905 (2020). https://doi.org/10.1103/PhysRevC.102.034905. arXiv:2004.00690 [nucl-th]
15. F.G. Gardim, G. Giacalone, M. Luzum, J.-Y. Ollitrault, Effects of initial state fluctuations on the mean transverse momentum. Nucl. Phys. A **1005**, 121999 (2021). https://doi.org/10.1016/j.nuclphysa.2020.121999. arXiv:2002.07008 [nucl-th]
16. F.G. Gardim, G. Giacalone, M. Luzum, J.-Y. Ollitrault, Thermodynamics of hot strong-interaction matter from ultrarelativistic nuclear collisions. Nat. Phys. **16**(6), 615–619 (2020). https://doi.org/10.1038/s41567-020-0846-4. arXiv:1908.09728 [nucl-th]
17. B. Bally et al., Imaging the initial condition of heavy-ion collisions and nuclear structure across the nuclide chart. arXiv:2209.11042 [nucl-ex]
18. S. Bhatta, C. Zhang, J. Jia, Higher-order transverse momentum fluctuations in heavy-ion collisions. Phys. Rev. C **105**(2), 024904 (2022). https://doi.org/10.1103/PhysRevC.105.024904. arXiv:2112.03397 [nucl-th]
19. Z. Lu, M. Zhao, J. Jia, Y. Zhou, Probe nuclear structure using the anisotropic flow at the Large Hadron Collider. arXiv:2309.09663 [nucl-th]
20. G. Giacalone, Many-body correlations for nuclear physics across scales: from nuclei to quark-gluon plasmas to hadron distributions. arXiv:2305.19843 [nucl-th]
21. G. Giacalone, Observing the deformation of nuclei with relativistic nuclear collisions. Phys. Rev. Lett. **124**(20), 202301 (2020). https://doi.org/10.1103/PhysRevLett.124.202301. arXiv:1910.04673 [nucl-th]
22. B. Bally, M. Bender, G. Giacalone, V. Somà, Evidence of the triaxial structure of ^{129}Xe at the Large Hadron Collider. arXiv:2108.09578 [nucl-th]
23. ALICE Collaboration, S. Acharya et al., Characterizing the initial conditions of heavy-ion collisions at the LHC with mean transverse momentum and anisotropic flow correlations. Phys. Lett. B **834**, 137393 (2022). https://doi.org/10.1016/j.physletb.2022.137393, arXiv:2111.06106 [nucl-ex]
24. B. Bally, G. Giacalone, M. Bender, The shape of gold. Eur. Phys. J. A **59**(3), 58 (2023). https://doi.org/10.1140/epja/s10050-023-00955-3. arXiv:2301.02420 [nucl-th]
25. N. Borghini, P.M. Dinh, J.-Y. Ollitrault, A New method for measuring azimuthal distributions in nucleus-nucleus collisions. Phys. Rev. C **63**, 054906 (2001). https://doi.org/10.1103/PhysRevC.63.054906. arXiv:nucl-th/0007063
26. J.-Y. Ollitrault, Measures of azimuthal anisotropy in high-energy collisions. Eur. Phys. J. A **59**(10), 236 (2023). https://doi.org/10.1140/epja/s10050-023-01157-7. arXiv:2308.11674 [nucl-ex]
27. A. Bilandzic, C.H. Christensen, K. Gulbrandsen, A. Hansen, Y. Zhou, Generic framework for anisotropic flow analyses with multiparticle azimuthal correlations. Phys. Rev. C **89**(6), 064904 (2014). https://doi.org/10.1103/PhysRevC.89.064904. arXiv:1312.3572 [nucl-ex]
28. Z. Moravcova, K. Gulbrandsen, Y. Zhou, Generic algorithm for multiparticle cumulants of azimuthal correlations in high energy nucleus collisions. Phys. Rev. C **103**(2), 024913 (2021). https://doi.org/10.1103/PhysRevC.103.024913. arXiv:2005.07974 [nucl-th]
29. J. Jia, Probing triaxial deformation of atomic nuclei in high-energy heavy ion collisions. Phys. Rev. C **105**(4), 044905 (2022). https://doi.org/10.1103/PhysRevC.105.044905. arXiv:2109.00604 [nucl-th]
30. ALICE Collaboration, K. Aamodt et al., Transverse momentum spectra of charged particles in proton-proton collisions at $\sqrt{s} =$ 900 GeV with ALICE at the LHC. Phys. Lett. B **693**, 53–68 (2010). https://doi.org/10.1016/j.physletb.2010.08.026, arXiv:1007.0719 [hep-ex]
31. P.J. Smith, A recursive formulation of the old problem of obtaining moments from cumulants and vice versa. Am. Stat. **49**(2), 217–218 (1995). http://www.jstor.org/stable/2684642
32. X.-N. Wang, M. Gyulassy, Energy and centrality dependence of rapidity densities at RHIC. Phys. Rev. Lett. **86**, 3496–3499 (2001). https://doi.org/10.1103/PhysRevLett.86.3496. arXiv:nucl-th/0008014
33. Z.-W. Lin, C.M. Ko, B.-A. Li, B. Zhang, S. Pal, A Multi-phase transport model for relativistic heavy ion collisions. Phys. Rev. C **72**, 064901 (2005). https://doi.org/10.1103/PhysRevC.72.064901. arXiv:nucl-th/0411110 [nucl-th]
34. B. Zhang, ZPC 1.0.1: a Parton cascade for ultrarelativistic heavy ion collisions. Comput. Phys. Commun. **109**, 193–206 (1998). https://doi.org/10.1016/S0010-4655(98)00010-1. arXiv:nucl-th/9709009
35. L.-W. Chen, C.M. Ko, System size dependence of elliptic flows in relativistic heavy-ion collisions. Phys. Lett. B **634**, 205–209 (2006). https://doi.org/10.1016/j.physletb.2006.01.037. arXiv:nucl-th/0505044 [nucl-th]
36. B.-A. Li, C.M. Ko, Formation of superdense hadronic matter in high-energy heavy ion collisions. Phys. Rev. C **52**, 2037–2063 (1995). https://doi.org/10.1103/PhysRevC.52.2037. arXiv:nucl-th/9505016 [nucl-th]
37. ALICE Collaboration, S. Acharya et al., "Anisotropic flow in Xe-Xe collisions at $\sqrt{s_{\rm NN}} = 5.44$ TeV", Phys. Lett. B **784**, 82–95 (2018). https://doi.org/10.1016/j.physletb.2018.06.059, arXiv:1805.01832 [nucl-ex]
38. C. Loizides, J. Nagle, P. Steinberg, Improved version of the PHOBOS Glauber Monte Carlo. arXiv:1408.2549 [nucl-ex]. [SoftwareX1-2,13(2015)]
39. ALICE Collaboration, S. Acharya et al., Skewness and kurtosis of mean transverse momentum fluctuations at the LHC energies. arXiv:2308.16217 [nucl-ex]

40. P. Bozek, Transverse-momentum-flow correlations in relativistic heavy-ion collisions. Phys. Rev. C **93**(4), 044908 (2016). https://doi.org/10.1103/PhysRevC.93.044908. arXiv:1601.04513 [nucl-th]
41. G. Giacalone, F.G. Gardim, J. Noronha-Hostler, J.-Y. Ollitrault, Correlation between mean transverse momentum and anisotropic flow in heavy-ion collisions. Phys. Rev. C **103**(2), 024909 (2021). https://doi.org/10.1103/PhysRevC.103.024909. arXiv:2004.01765 [nucl-th]
42. X.-N. Wang, M. Gyulassy, HIJING: A Monte Carlo model for multiple jet production in pp, pA and AA collisions. Phys. Rev. D **44**, 3501–3516 (1991). https://doi.org/10.1103/PhysRevD.44.3501